doi: 10.1038/nature00817

Supplementary Information

"Greenhouse gas emission targets for limiting global warming to 2°C"

Malte Meinshausen[1], Nicolai Meinshausen[2], William Hare[1,3], Sarah C. B. Raper[4], Katja Frieler[1], Reto Knutti[5], David J. Frame[6,7], Myles R. Allen[7]

[1] *Potsdam Institute for Climate Impact Research, Telegraphenberg, 14412 Potsdam, Germany;*
[2] *Department of Statistics, South Parks Road, University of Oxford, Oxford, OX1 3TG, United Kingdom;*
[3] *Climate Analytics, Telegraphenberg, 14412 Potsdam, Germany;*
[4] *Centre for Air Transport and the Environment, Manchester Metropolitan University, Chester Street, Manchester M1 5GD, United Kingdom;*
[5] *Institute for Atmospheric and Climate Science, ETH Zurich, 8092 Zurich, Switzerland;*
[6] *Smith School of Enterprise and the Environment, University of Oxford, Oxford, OX1 2BQ, United Kingdom;*
[7] *Department of Physics, University of Oxford, Parks Road, Oxford, OX1 3PU, United Kingdom;*

CONTENTS

COUPLED CARBON CYCLE CLIMATE MODEL

We use the reduced complexity coupled carbon cycle climate model (MAGICC 6.0), that uses (hemispheric) emissions of greenhouse gases, aerosols, and tropospheric ozone precursors as its main inputs and calculates atmospheric concentrations, radiative forcings, surface air temperatures, and ocean heat uptake. MAGICC has been used extensively in past IPCC Assessment reports to emulate higher complexity models. MAGICC 6.0 is able to closely emulate both IPCC AR4 CMIP3 AOGCMs and C4MIP carbon cycle models.[1] Thus, we use MAGICC 6.0 here both for future climate projections based on historical constraints and for emulating more complex AOGCMs or carbon cycle models.

The model contains many parameters whose values are uncertain. We looked at the impact of 82 parameters on model behaviour. They include the main sources of uncertainty for temperature projections, such as equilibrium climate sensitivity, dependence of the effective climate sensitivity on forcing, ocean diffusivity and its dependence on the ocean's vertical warming gradient, forcing of CO_2 at doubled concentrations, the indirect aerosol forcing in 2005 and the respective contributions from SO_x, NO_x, black and organic carbon emissions. Nine parameters are crucial for the simple energy balance upwelling-diffusion-entrainment climate model in MAGICC 6.0, while 33 parameters are related to the different gas-cycles in MAGICC (not considering the 18 carbon cycle parameters that are calibrated separately[1] in order to emulate individual C4MIP carbon cycle models) as well as global radiative forcing parameters. The remaining parameters that were varied relate to the relative patterns of the radiative forcings across the four spatial boxes, Northern hemisphere land (NL) and ocean (NO) and Southern hemisphere land (SL) and ocean (SO) (Table S1). All 82 parameters are summarized in the vector $\boldsymbol{\Theta}$.

OBSERVATIONAL CONSTRAINTS

As one set of observational constraints, we use yearly averaged temperatures in our four grid boxes (Northern and Southern hemisphere land and ocean) as provided by Brohan et al.[2] for the years 1850-2006. We arrange those measurements in a 628-dimensional vector **T**. Uncertainty in these measurements comprises both an independent error, reflecting measurement uncertainties, and up to two potential bias sources, reflecting urbanisation effects and thermometer exposure changes. The independent measurement errors and the bias errors are assumed to follow 'skewed normal' distributions with appropriate time-varying variance. Here, a random variable X is called 'skewed normal', if $\log(X\text{-}c)$ has a Gaussian distribution with mean μ and variance σ^2. This allows a continuous approximation between a Gaussian distribution of X and skewed log-normal distributions – by making an appropriate choice for c. The constants c, μ and σ are chosen so that the reported quantiles of the distribution of X are matched. They are uniquely determined this way. An exception is the possible urbanization bias over land areas. In this case, we use a truncated normal distribution, whose mass on the negative axis is concentrated at zero. The respective space-time dependency is obtained from Brohan et al.[2]. The contributions from each of the two bias sources are assumed to be perfectly correlated between different years and land or ocean areas, respectively. The first bias source is assumed to be independent of the second bias source, though.

Internal climate variability has to be taken into account when comparing model results under various parameter settings to observed surface temperatures. We use the full-length control runs of all AOGCMs runs available at PCMDI (http://www-pcmdi.llnl.gov/, as of mid 2007) to assess internal variability. For each AOGCM, we estimate the 628x628 dimensional covariance matrix Σ of the observations **T** resulting from measurement error *and* internal climate variability under the constraint of stationarity of the temperature time series.

Even if we were assuming a multivariate normal distribution for the internal climate variability of **T** (which we do not), we are still faced with estimating a high-dimensional covariance matrix Σ and using its inverse in the calculation of the likelihood. As the control runs are of limited length, the associated structural errors in the estimate of internal climate variability can affect the inverse of Σ and hence the likelihood substantially. We address this by projecting the 628-dimensional vector of temperature measurements onto a low-dimensional subspace. Optimizing a signal-to-noise ratio for this projection is dangerous, as discussed in Allen & Tett[3], as one is then likely to pick up directions which do not show sufficient variance in the GCM control runs. As we also want to avoid projecting onto dimensions that cannot be modelled by MAGICC, we simply search for the m-dimensional projection (with low m) which best preserves the MAGICC signal. To this end, we draw 5,000 parameters **Θ** from the prior distribution of Θ, compute the MAGICC output **T** under all these parameter sets and perform a PCA analysis. We choose m so that 99.95% of the MAGICC variance is preserved and find that m=8 is sufficient. Our findings are insensitive to this choice. We then find the mx628-dimensional matrix P_m, which corresponds to the projection of **T** onto the space spanned by the first m PCA components. The likelihood is finally based on the m-dimensional vector $\mathbf{T_m}=P_m\mathbf{T}$ instead of the 628-dimensional vector **T**. Note that each PCA component is spatio-temporal in nature to achieve maximum dimensionality reduction while retaining most of the signal in MAGICC. We now assume that the internal variability of $\mathbf{T_m}$ has a Gaussian distribution (which is more plausible than assuming a Gaussian distribution for T directly, due to the involved projection) and estimate the mxm-dimensional covariance matrix Σ_m from the data set as $P_m^T \Sigma P_{m,,}$ where Σ is the previously derived covariance matrix of the observations.

Ocean heat uptake is only considered via its linear trend Z_1 of +0.3721(1-sigma: ±0.0698) 10^{22} J/yr for the heat content trend over 1961 to 2003 up to 700m depth[4]. See Figure S2 for the match between the constrained model results and the observational data by Levitus et al.[5] as well as more recent results by Domingues et al.[4].

Radiative forcing estimates as listed in Forster et al. (Table 2.12 therein)[6] provide an additional set of 17 constraints $Z_2,...,Z_{18}$ (Table S2). The error of 14 of these radiative forcing estimates is assumed to have a Gaussian distribution, as the 5% and 95% quantiles of the error distribution given in Forster et al.[6] do not hint towards skewness of the error. The remaining 3 observational constraints are modelled by a 'skewed normal' (see above). Using a Gaussian distribution instead yields very similar results, though, and all conclusions are not affected by the details of the distribution chosen. All radiative forcing uncertainties are assumed to be independent.

Given that MAGICC 6.0 has substantially more freedom to change the effective climate sensitivity over time[1] than what is observed from AOGCM diagnostics, we introduce another constraint Z_{19}. This constraint limits the ratio of the 21st century change in effective climate sensitivity, expressed by the ratio of average effective climate sensitivities in the periods 2050-2100 and 1950-2000. Based on AOGCM CMIP3 model emulations[1], we derive a distribution for our constraint with a median at 1.23 and a 90% range between 1.06 to 1.51 under the SRES A1B scenario.

LIKELIHOOD ESTIMATION

To calculate the likelihood, the observations are split into the projected temperature observations T_m and the remaining observational constraints $Z_1,...,Z_{19}$. Let f be the density of temperature observations under a given parameter setting Θ, taking into account both the measurement errors and internal climate variability. Let h_k, k=1,…,19, be the density functions of the remaining observational constraints. Under independence of $Z_1,...,Z_{19}$ and T, the likelihood L(Θ) of model parameters Θ is given by:

$$L(\Theta) = f(T_m|\Theta) \prod_{k=1}^{19} h_k(Z_k|\Theta)$$

We follow mostly a Bayesian approach. A prior distribution π over the parameter vector Θ is specified in various ways as discussed further below - see Table S1 for prior assumption on key parameters. Given the *a priori* assumption, we are able to specify the posterior distribution g(Θ) of the parameters as proportional to the product of the likelihood L(Θ) and the prior π(Θ):

Sensitivity to the chosen prior and a comparison with frequentist inference are discussed further below. For frequentist inference, we work directly with the likelihood.

MODEL SAMPLING

To draw models from the posterior distribution g(Θ), a Markov Chain Monte Carlo approach is used, using a standard Metropolis-Hastings algorithm with adaptive step sizes to attain an average acceptance rate of 60%. 45 Markov chains are run in parallel for 75,000 iterations each. Adjusting for a burn-in time of 20,000 iterations, and retaining only every 30th model, to decrease dependence between successive models, a total of 82,500 models are drawn from the posterior distribution. For probabilistic forecasts, 600 models with maximal spacing in this set of 82,500 models are retained and combined randomly with one of the 10 parameter sets used for emulating individual C4MIP carbon cycle models[1]. Global mean surface temperatures for the years 1765-2100 are derived under these 600 combinations of climate, radiative forcing, gas-, and carbon-cycle parameterisations.

REPRESENTING PUBLISHED CLIMATE SENSITIVITY DISTRIBUTIONS

Apart from the frequentist likelihood confidence intervals, we represent the wide range of literature studies on Bayesian climate sensitivity (CS) distributions by adapting the (inherently subjective) Bayesian priors for climate sensitivity. For a full list of studies shown in Fig.1 of the main manuscript, see Table S4 below. In these studies, climate sensitivity is constrained by, for example, historical data on millennial[7] and centennial timescales[8-10], or current climatologies[11,12]. Specifically, we change the prior for climate sensitivity such that a match between our posterior PDF of climate sensitivity and the posterior distribution in the considered studies is achieved. For each new prior, the models selected for further analysis are obtained by drawing, with replacement, 600 models from the original 82,500 models, where the probability of drawing a particular model is proportional to the ratio of the posterior density under the new prior and the posterior under a uniform prior. We leave the prior over all other parameters unchanged. Furthermore, we restrict the default 0-20K range of the CS prior to 0 to 10K as this is the reported range for most CS distributions in the literature. The range of CS between 0 and 10 is divided into 50 bins of equal width and the prior distribution

over CS is chosen piecewise constant for each bin, using values such that the posterior distribution matches the given posterior distribution as closely as possible, by minimizing the maximal absolute difference between the target posterior and the achieved posterior of CS. The sensitivity of the results is shown in Figure 3 of the main paper.

For illustrative purposes, we chose the climate sensitivity distributions by Frame et al. (2006)[13] as our default, given that this distributions resembles most closely the IPCC AR4 estimate for climate sensitivity (best-estimate 3°C with likely range between 2.0 to 4.5°C). Specifically, our criterion for measuring the proximity towards this IPCC AR4 'consensus' estimate is the maximal absolute deviation of the median from 3°C, the 10% quantile from 2.0°C and the 90% quantile from 4.5°C. Frame et al. (2006) UniTCR is the only distribution for which the deviation is smaller than 0.2°C for all three reference points. We recognize that this is only one criterion out of many possible ones.

ROBUSTNESS TESTS

We tested the sensitivity of our results due to the limited sampling size, which we chose as 600 by default. With a single scenario (HALVED-BY-2050), we calculated the probability of exceeding 2°C twenty-five times using sample sizes of 100, 500 and 1,000. As a result, the estimated probability of exceeding 2°C varied by up to ±7.5%, ±6%, and ±5%, respectively.

We tested that results are rather insensitive to the number of principal components (PCs) retained. We consider only up to 8 PCs as the additional variance among the MAGICC model runs, which is explained by PCs beyond the 7th or 8th component, is negligible for all practical purposes and might rather introduce biases or noise.

The AOGCM from which the control run was chosen to estimate the covariance structure on our reduced-dimensional temperature observations had some influence on the results, approximately ±10% under a HALVED-BY-2050 and SRES B1 scenario.

We performed sensitivity tests as well using previous ocean heat content data with a lower trend, as given in Levitus et al.[5], and adjusted uncertainties as given in Tomassini et al.[14], i.e. +0.2284 (1-sigma: 0.1946 to 0.2622) 10^{22} J/yr over 1957 to 1996 for the heat content changes up to 700m depth. The 2°C exceedance probabilities for a given emission budget are affected by approximately up to +5%.

In addition, we tested the influence of the carbon cycle uncertainties on our results. Choosing an emulation of the model with the highest carbon cycle feedback within the C4MIP intercomparison (HADLEY)[1] (rather than sampling randomly from 10 different C4MIP emulations) resulted in 2°C exceedance probabilities (as shown in Figure 3a) to increase by approximately +15% for scenarios below 2,200 $GtCO_2$ of cumulative 2000-2049 CO_2 emissions.

EMISSION SCENARIOS

In this study, we complement the multi-gas IPCC SRES and EMF-21 scenarios with a large ensemble of multi-gas EQW pathways, which replicate most characteristics of the SRES and EMF scenarios. Prescribing simple CO_2 pathways and following a regression of CO_2 concentrations and total radiative forcing (as has been employed by IPCC AR4 WGIII[15]) is too simplistic for the purposes of the analyses conducted here for several reasons: First, the regression shown in Fig. 3.16 of IPCC AR4 WGIII is problematic, as it effectively implies an increasing non-CO_2 radiative forcing contribution for the lower scenarios (Figure S6). Second, the regression between year 2100 CO_2 concentrations and year 2100 total radiative forcing

does not necessarily reflect the forcing shares important for calculating maximal temperatures. Third, the CO_2 and non-CO_2 forcing contributions for the scenarios need to be calculated from internally and historically consistent sets of emissions, as we will otherwise encounter multiple inconsistencies between our historical constraining approach and future projections. For example, we assume here, in line with Hansen et al.[16], that in addition to SO_x, nitrate aerosols, black and organic carbon contribute to the indirect aerosol effect, which results overall in a more negative forcing contribution throughout the 21st century compared to an approach based on SO_x emissions only. That is why – in average – our non-CO_2 forcing contributions in year 2100 tend to be lower than implied by the data points shown in Fig. 3.16 of IPCC AR4 WGIII (Figure S6). Overall, the EQW pathways replicate most of the characteristics of multi-gas scenarios quite well. This is due to the fact that emissions of the EQW pathways are a direct derivative of a large ensemble of these multi-gas scenarios, using the Equal-Quantile-Walk (EQW) method[17]. For a comparison between EQW and multi-gas scenarios from the literature for a key set of characteristics, see Figure S5.

We drew 948 EQW pathways from a one million member ensemble of EQW pathways we generated with all permutations of 10 possible reduction or increase rates (-6%, -5%, -4%, -3%, -2%, -1%, 0%, +1%, +2%, +3%) at each of the 5 chosen branching points (2010, 2015, 2020, 2030, 2050). Our first criterion is a curvature limitation to reflect some sense of realistic maximum rates of change, so that from one branching point to the next, the maximum difference in annual increases or reductions is 3 percentage points. The second criterion is that pathways, which started to decline (≤-1%/yr reduction), will not rise again – reflecting a general property of most mitigation scenarios. The third criterion only accepts those pathways with cumulative emissions less than 7,333 $GtCO_2$ between 2000 and 2099, as higher pathways are not of interest for determining the probability of exceeding 2°C. Following these criteria, we keep 6004 EQW pathways. Of these, we sample one in every six paths at random in order to limit the total number of necessary model runs, as each scenario is run with 600 parameter settings.

SENSITIVITY RESULTS IN REGARD TO EQW EMISSION PATHWAYS

While the multi-gas characteristics of the EQW emission pathways are derived from and in line with literature scenarios (see Figure S5), we test the dependence of our results with regard to the shape parameters of our EQW ensemble. In particular, we allow more degrees of freedom for changes in reduction rates after 2030. Specifically, we design another EQW ensemble with the following shape definitions: (a) there are 5 possible reduction or increase rates (-6%, -4%, -1%, 2%, 4%), (b) six branching points (2010, 2020, 2030, 2040, 2050, 2060), (c) and we allow a maximum difference in annual increases or reductions of 10 percentage points. This results in 1,573 EQW emission pathways, from which we randomly select one in every four scenarios. The results, as shown in Figure S4, suggest that even with these larger degrees of freedom regarding the shape of the emission profiles, our main conclusions are robust. These sensitivity runs roughly sample the same space within the probability versus cumulative emissions plot as our default ensemble of EQW emission pathways.

Additionally, we investigate the effect of setting all post 2050 emissions within this sensitivity ensemble of emission pathways to zero, thereby retrieving a lower bound on the exceedance probability related to pre-2050 emissions (see note "1" in Figure S4). Note, that this lower bound could be undercut by scenarios that imply negative post-2050 emissions. This is indicated by the multi-gas EMF-21 scenario (IMAGE 2.6), which assumes negative fossil CO_2 emissions after 2070 (see note "3" in Figure S4). Another peculiarity is that at the lower end,

the immediate cessation of emissions in year 2050 will induce slightly higher 2°C exceedance probabilities, which is due to a sudden drop of negative forcing related to aerosol emissions[18] (see note "2" in Figure S4). Finally, note that the ensembles of EQW pathways created here are intended to sample the emission space, which has a likely probability of achieving a 2°C target. Thus, the high-exceedance probability areas of the high reference scenarios with continuing high emissions during the second half of the 21st century are not populated by the EQW ensembles (see note "4"in Figure S4).

SMOOTHING FILTER USED FOR PROBABILITIES

The smoothed lines in Fig. 3a in the main paper and Fig. S1 indicate the probabilities of exceeding 2°C. These lines are derived by applying a locally weighted scatter plot using least squares linear polynomial fitting with smoothing windows of 30% over all individual data points.

FOSSIL FUEL RESERVES

The proven recoverable reserves are those fossil fuels that are recoverable in the future under present and expected local economic conditions with existing and available technology. Note that fossil fuel *resources*, the potentially accessible fossil fuel in the ground, are substantially larger than the *proven recoverable reserves*. We estimate potential emissions from proven recoverable reserves of fossil fuels, as shown in Fig 3b and Table S2, according to $E = R \times V \times C \times f$, where E are the potential emissions ($GtCO_2$), *R* the proven recoverable reserves (Gg), *V* the net calorific value (TJ/Gg), *C* the carbon content (tC/TJ) and *f* a conversion factor ($GtCO_2$/tC).

Our median estimates of proven recoverable fossil fuel reserves (R) are based on the World Energy Council (WEC) Survey of Energy Resources of 2007[19], with the exception of the non-conventional oil reserves which are taken as the median between the BP Statistical Review of World Energy[20] and the German Federal Institute for Geosciences and Natural Resources 2006 resource survey[21]. Potential emissions are estimated using IPCC 2006 default net calorific values (V) and carbon content emission factors (C)[22] (Table 1.2 and Table 1.3 therein).

We estimate the 80% uncertainty range in these reserve estimate as being ±10% the WEC[19] estimates or the range of estimates in the literature[20,21,23-26], whichever is greater, for individual classes of reserves. We combine these reserve uncertainties with the provided 95% ranges of calorific values and emission factors for each class of energy reserves[22]. We fit 'skewed normal' distributions (cf. section 2 above) for the reserve *R*, calorific value *V* or carbon content *C*. For non-conventional oil, we assume a uniform distribution. We assume independence between *R*, *V* and *C* and apply a 10,000 member Monte Carlo algorithm to estimate uncertainties in emissions from proven recoverable fossil fuel reserves (Table S2).

LANDUSE EMISSIONS AND EMISSIONS OF OZONE DEPLETING SUBSTANCES

As contribution to total CO_2 emissions, we show in Fig. 3b the 80% range (-35 to 248 $GtCO_2$) and median (24 $GtCO_2$) of cumulative CO_2 emissions from landuse activities over the period 2007 to 2049 as indicated across 50 IPCC SRES[27] scenarios. For all our climate model runs, we assume emissions of ozone depleting substances controlled by the Montreal Protocol to follow

the A1 baseline scenario from WMO 2006 Ozone Assessment[28], which assumes compliance with provisions of the Montreal Protocol, and its amendments.

COUNTRIES CALLING FOR LIMITING WARMING TO 2°C OR BELOW

The European Union, which now comprises 27 countries, has a position adopted at head of Government level calling for global warming to be limited to a maximum increase of 2°C relative to preindustrial levels[29]. The Alliance of Small Island States and the Least Developed Country group called for warming to be limited to 1.5°C at the 14th Conference of the Parties to the United Nations Framework Convention on Climate Change in Poznan, Poland, December 2008[30]. Furthermore, Norway[31], South Africa[32], Switzerland[33] and Iceland[34], as well as Costa Rica, El Salvador, Honduras, Nicaragua, and Panama[35] called for the global temperature increase to be limited to below 2°C. These groups comprise together a total of 110 countries and represent approximately 20% of the World's population in 2005[36].

FIGURES S1 TO S6

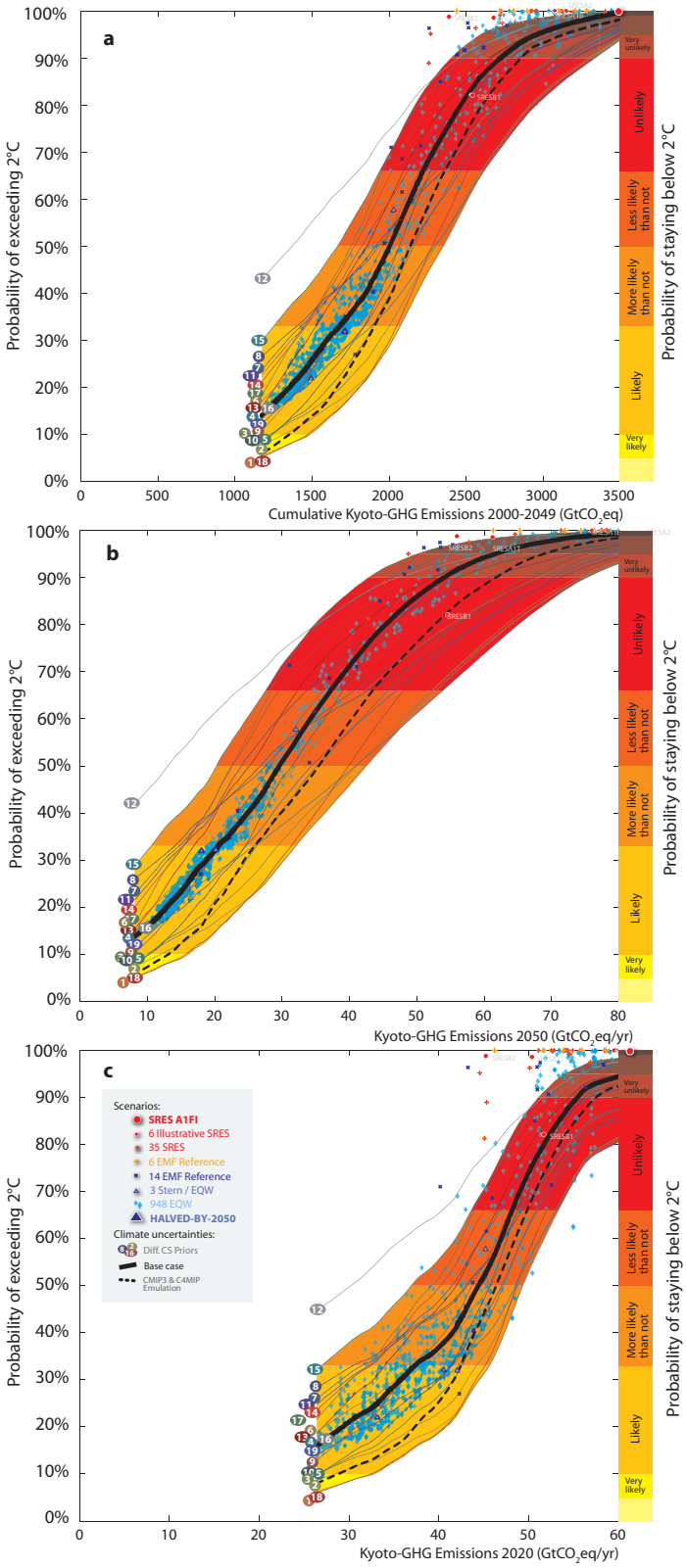

Figure S1 | Probabilities of exceeding 2°C for various emission indicators: **a**, cumulative Kyoto-gas emissions 2000-2049; **b**, 2050 Kyoto-gas emissions: **c**, 2020 Kyoto-gas emissions. Otherwise as Figure 3 in the main paper. In panel c the wide vertical spread of individual scenarios' exceedance probabilities (dots) indicates that 2020 emissions are a relatively poor indicator for maximum warming. This contrasts with 2050 Kyoto-gas emissions (b), for which the narrow vertical spread of individual scenarios' exceedance probabilities suggests that this indicator is well suited for the chosen class of scenarios. The dashed vertical lines in panel b indicate halved 1990 Kyoto-gas emissions and the bold line indicates the respective range of exceedance probabilities derived from our default constraining as well as the emulation of other studies' climate sensitivity distributions.

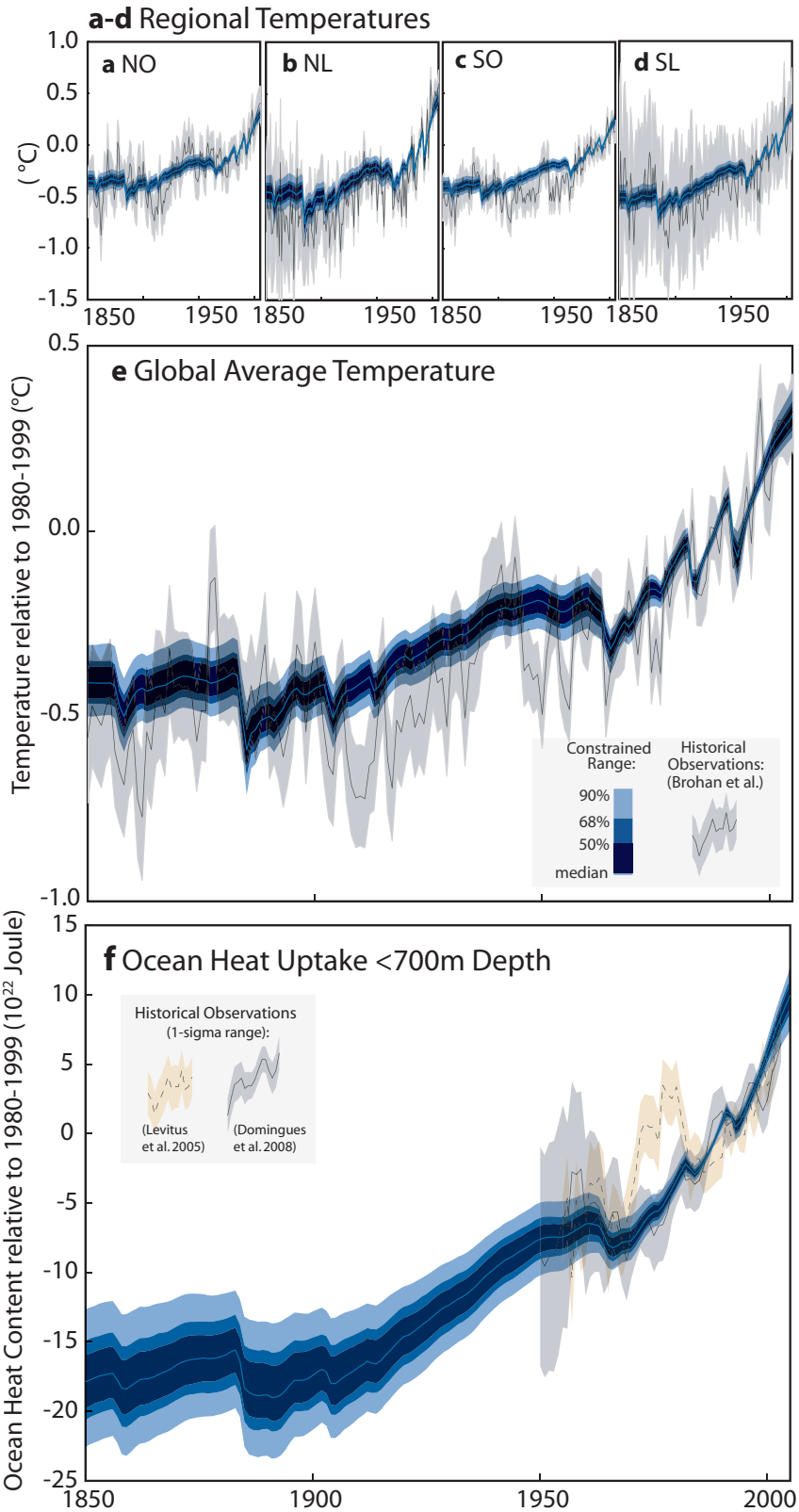

Figure S2 | Observations and constrained model results for temperatures and ocean heat content changes. a, Modelled average surface temperatures using the illustrative default case and observed[2] data with 95% uncertainty range for northern hemisphere ocean; **b**, northern hemisphere land; **c**, southern hemisphere ocean; **d**, southern hemisphere land; **e**, the global average; **f**, Modelled and observed[4,5] changes in ocean heat content up to 700m depth. The regional temperatures and the linear trend of ocean heat uptake[4] over 1961 to 2003 were used to constrain the climate model parameter space. The MAGICC 6.0 results based on our illustrative default are shown in blue. The agreement between observed and modelled ocean heat uptake up to 300m or 3,000m depth[5] is similar as shown here for 700m.

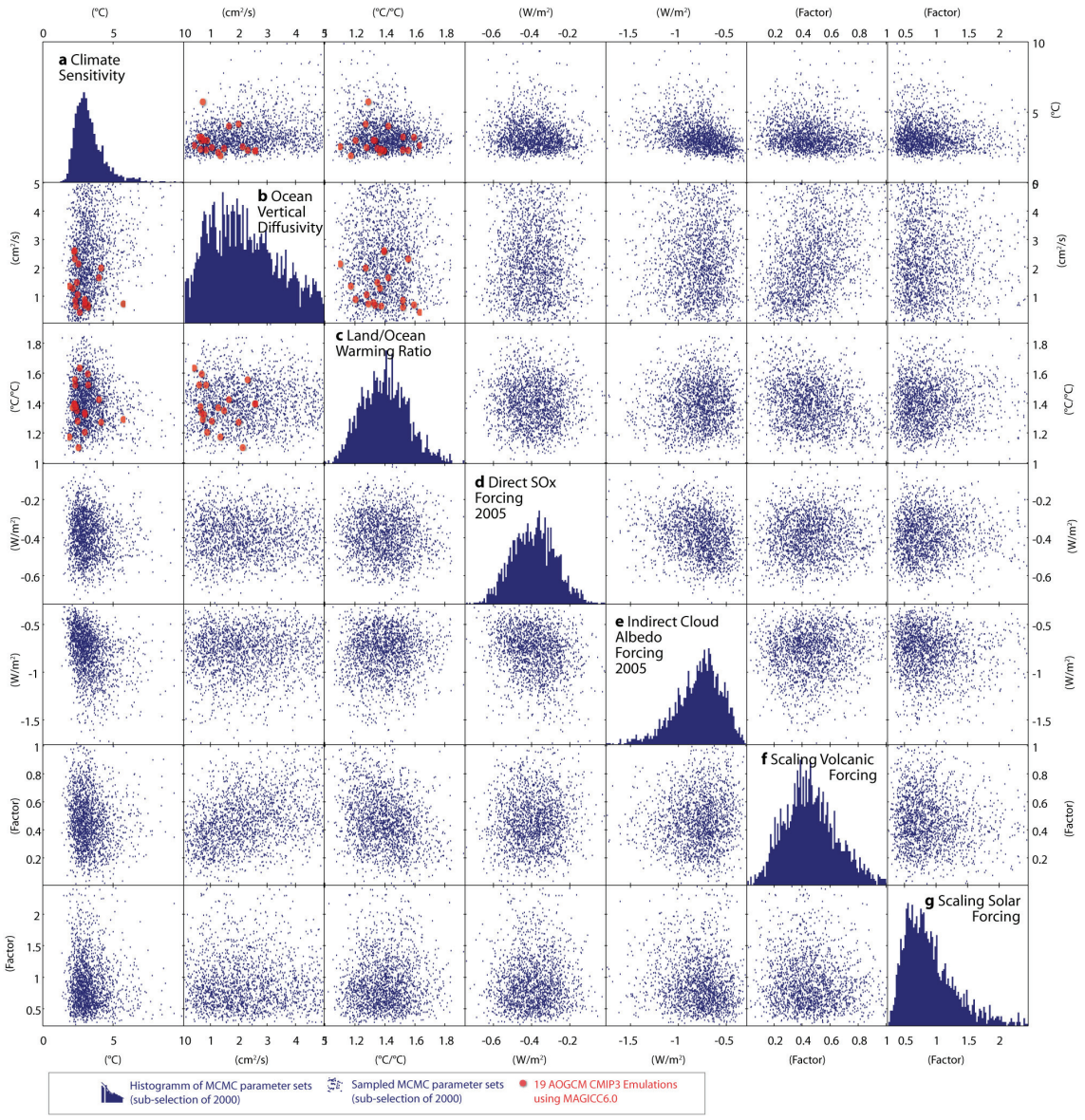

Figure S3 | Joint distribution of seven key MAGICC parameters, as example of the 82-dimensional parameter space we constrained. a-g, Histograms of parameters are provided in the diagonal, and 2,000 randomly drawn parameter sets are indicating the joint distributions (illustrative default) between any two parameters in the off-diagonal scatter plots. Parameter sets that were calibrated to emulate 19 CMIP3 AOGCMs are provided as red dots in the off-diagonal scatter plots of the parameters climate sensitivity (a), ocean vertical diffusivity (b) and equilibrium land-ocean warming ratio (c).

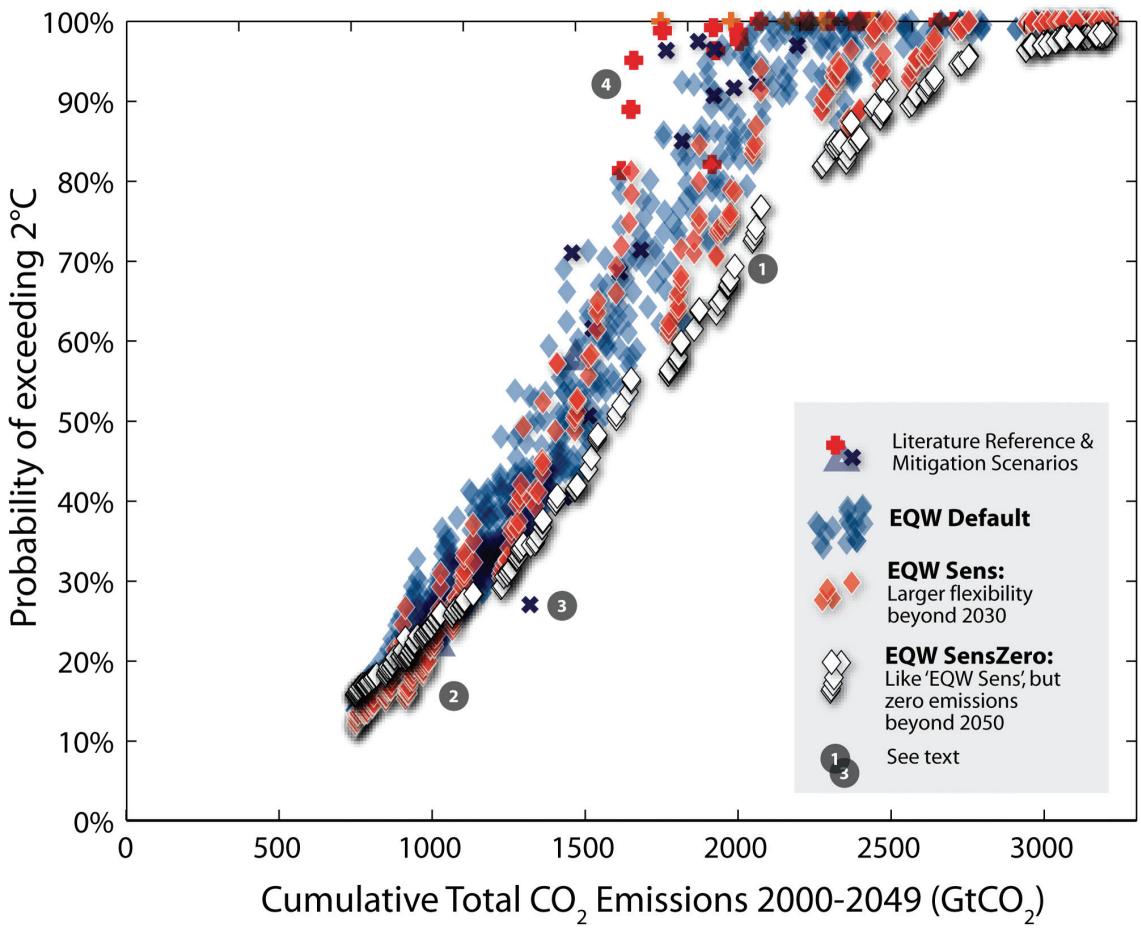

Figure S4 | Sensitivity test for the shape parameters of the EQW emission pathway ensemble. Probability of exceeding 2°C warming as a function of cumulative total CO_2 emissions are shown for different sets of EQW pathways. See text for explanations.

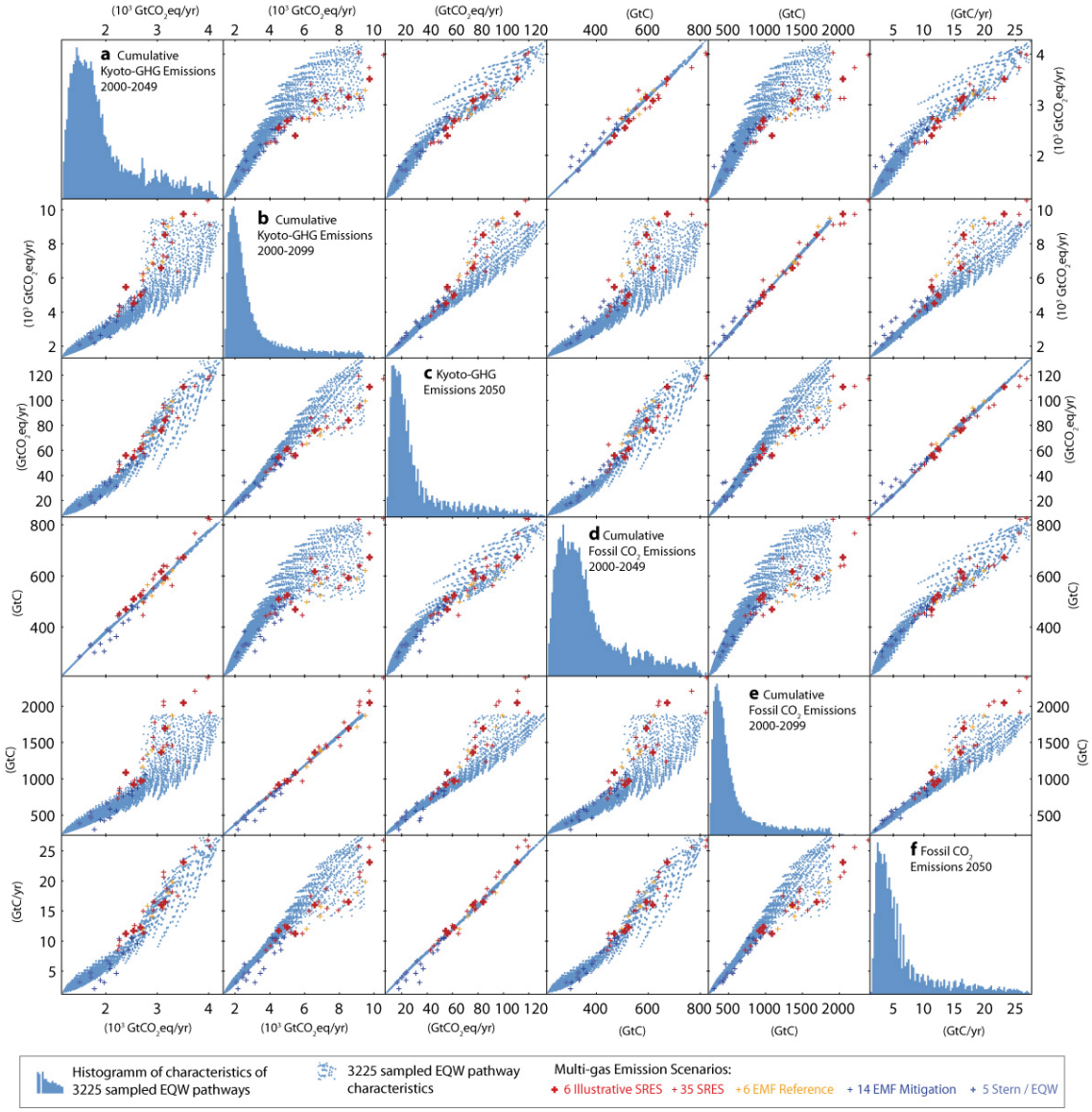

Figure S5 | Comparison of key emission scenario characteristics between EQW and multi-gas IPCC SRES, EMF-21 scenarios. a, cumulative Kyoto-GHG emissions between 2000 and 2049; **b**, cumulative Kyoto-GHG emissions between 2000 and 2099; **c**, single-year Kyoto-GHG emissions for 2050; **d,e,f**, same as a,b,c but for fossil & industrial CO_2 emissions. SRES and EMF-21 scenarios are shown as red, orange and dark blue dots and the default EQW pathway ensemble used in this study is shown as bright blue dots in off-diagonal plots and histograms on the diagonal.

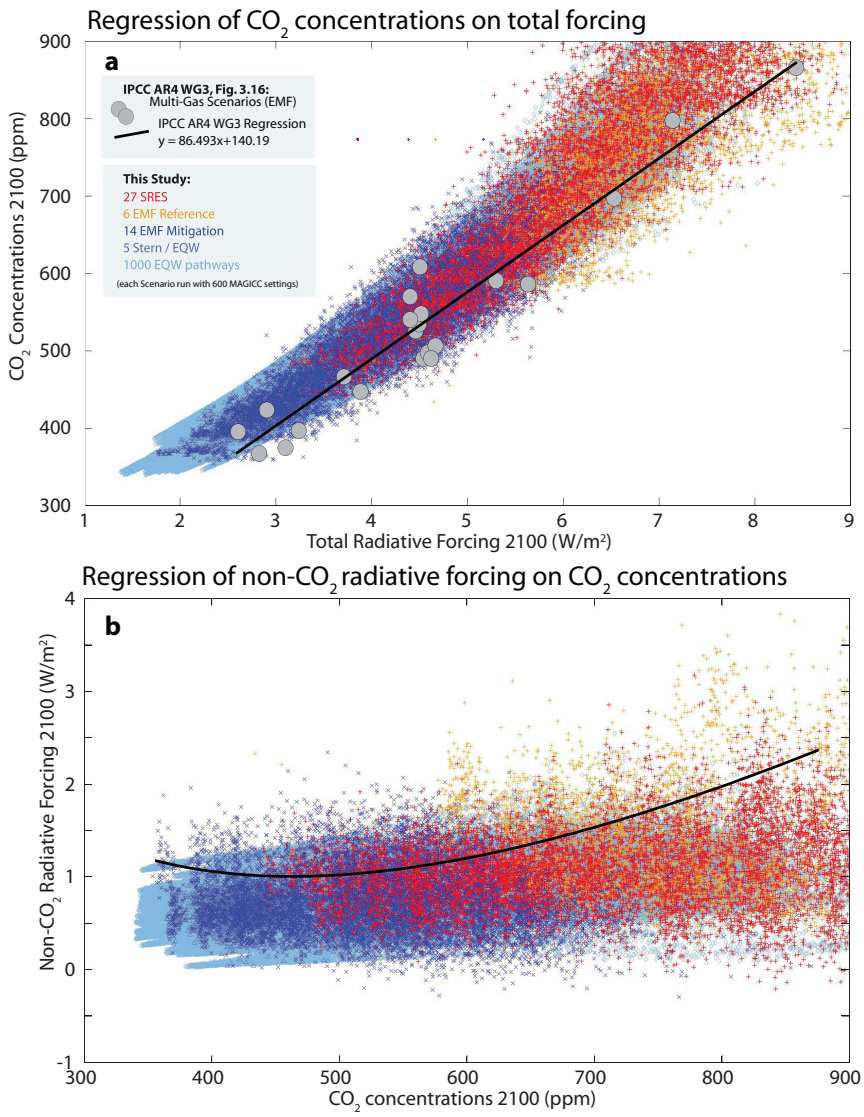

Figure S6 | Regression of CO_2 concentrations in year 2100 to net total radiative forcing. a, CO_2 concentrations vs. total radiative forcing for emission scenarios used in this study (small colored dots), and the stabilization scenarios (grey dots) including the linear regression (black line) as shown in Fig. 3.16 of Working Group III, IPCC AR4[15]; **b**, CO_2 concentrations vs. non-CO_2 radiative forcing in year 2100, including the regression line from a. The linear regression shown in a is not linear when plotted in panel b due to the non-linear concentration to forcing relationship of CO_2. The IPCC AR4 WGIII regression hence includes the implicit assumption of higher non-CO_2 forcing, the more CO_2 concentrations are reduced below about 475ppm (cf. black bold line bending upwards towards low concentration levels in panel b). Another difference of our study is that – on average – our results suggest lower non-CO_2 radiative forcing contributions in 2100 than implied by the WGIII regression line (see text).

TABLES S1 TO S4

Table S1 | Climate, gas-cycle and radiative forcing parameters in MAGICC 6.0, which have been varied for the historical constraining. Uniform priors have been applied between the given min-max boundaries. Standard mid values provided for illustrative purposes only. Table continued on next page.

No.	Parameter	Region	Description	Unit	Min	Max	Standard
Climate Model Parameters							
1	CORE_CLIMATESENSITIVITY	GL	Climate Sensitivity	K	0.050	20.000	3.000
2	CORE_VERTICALDIFFUSIVITY	GL	Vertical diffusivity ocean	cm^2s^{-1}	0.100	5.000	2.300
3	CORE_AMPLIFY_OCN2LAND_HEATXCHNG	GL	Amplification factor for ocean to land heat transport		1.000	1.500	1.000
4	CORE_FEEDBACK_QSENSITIVITY	GL	Dependence of feedback factors on forcing	1E3 Km^2W^{-1}	0.000	0.075	0.038
5	CORE_HEATXCHANGE_LANDOCEAN	GL	Heat exchange coefficient land ocean	$Wm^{-2}K^{-1}$	0.250	6.000	1.000
6	CORE_HEATXCHANGE_NORTHSOUTH	GL	Heat exchange coefficient north south	$Wm^{-2}K^{-1}$	0.250	6.000	1.000
7	CORE_RLO	GL	Ratio land ocean warming		1.000	2.000	1.300
8	CORE_UPWELL_THRESH_TEMP_NH	GL	Temperature threshold at which minimum meridional overturning reached	K	2.000	20.000	8.000
9	CORE_VERTICALDIFF_TOP_DKDT	GL	Dependence of vert. diffusivity on ocean warming gradient	$cm^2s^{-1}K^{-1}$	-1.000	0.000	-0.500

Table S1 (continued).

No.	Parameter	Region	Description	Unit	Min	Max	Standard
Radiative Forcing & Gas-cycle Parameters							
10	CORE_DELQ2XCO2	GL	Forcing for doubled CO_2	W/m^2	3.310	4.110	3.710
11	CH4_ADDEDSTRATH2O_PERCENT	GL	Forcing due to strat. H_2O due to methane		0.020	0.200	0.050
12	CH4_RADEFF_WM2PERPPB	GL	Rad. forcing efficiency CH_4	$W/m^2/ppb$	0.024	0.054	0.036
13	CH4_SCALEOHSENS	GL	OH sensitivity of methane lifetime		0.500	1.500	1.000
14	CH4_TAUTEMPSENSITIVITY	GL	Temperature sensitivity of methane lifetime	yr/K	0.016	0.047	0.032
15	CLOUD_WEIGHT_BC	GL	Contribution black carbon to indirect aerosol forcing		0.000	0.020	0.020
16	CLOUD_WEIGHT_NOX	GL	Contribution nitrates to indirect aerosol forcing		0.000	0.080	0.080
17	CLOUD_WEIGHT_OC	GL	Contribution organic carbon to indirect aerosol forcing		0.000	0.130	0.130
18	N2O_RADEFF_WM2PERPPB	GL	Rad. forcing efficiency N_2O	$W/m^2/ppb$	0.100	0.160	0.120
19	N2O_TAUINIT	GL	N2O initial lifetime	yrs	110.000	130.000	120.000
20	RF_BCB_DIR_WM2	GL	Black carbon direct forcing from biomass burning 2005	W/m^2	0.000	0.500	0.200
21	RF_BCI_DIR_WM2	GL	Black carbon direct forcing from fossil fuel burning 2005	W/m^2	0.000	0.500	0.200
22	RF_BCSNOW_ALBEDO_WM2	GL	Black carbon on snow albedo forcing 2005	W/m^2	0.000	0.400	0.100
23	RF_CLOUD_ALBEDO_AER_WM2	GL	Ind. aerosol / cloud albedo forcing 2005	W/m^2	-1.750	0.000	-0.700
24	RF_EFFICACY_CLOUD_ALBEDO	GL	Efficacy of cloud albedo forcing (accounting for scaling due to cloud lifetime changes)		1.000	2.000	1.500
25	RF_FGASSUM_SCALE	GL	Scaling factor for fluorinated gases forcing		0.875	1.100	1.000
26	RF_LANDUSE_ALBEDO_WM2	GL	Radiative forcing 2005 due to landuse albedo	W/m^2	-0.600	0.100	-0.200
27	RF_MHALOSUM_SCALE	GL	Scaling factor for forcing of substances controlled under the Montreal Protocol		0.875	1.100	1.000
28	RF_MINERALDUST_DIR_WM2	GL	Rad. forcing due to mineral dust 2005	W/m^2	-0.500	0.200	-0.100
29	RF_NOXB_DIR_WM2	GL	Direct rad. forcing due to NO_x from biomass burning 2005	W/m^2	-0.400	0.100	-0.100
30	RF_NOXI_DIR_WM2	GL	Direct rad. forcing due to NO_x from fossil fuel burning 2005	W/m^2	-0.400	0.000	-0.100
31	RF_OCB_DIR_WM2	GL	Direct rad. forcing due to organic carbon from biomass burning 2005	W/m^2	-0.500	0.000	-0.200
32	RF_OCI_DIR_WM2	GL	Direct rad. forcing due to organic carbon from fossil fuel burning 2005	W/m^2	-0.200	0.000	-0.050
33	RF_SOLAR_SCALE	GL	Scaling factor for solar forcing	W/m^2	0.100	2.500	0.657
34	RF_SOXB_DIR_WM2	GL	Direct rad. forcing due to sulphate aerosols from biomass burning 2005	W/m^2	-1.000	0.000	-0.400
35	RF_SOXI_DIR_WM2	GL	Direct rad. forcing due to sulphate aerosols from fossil fuel burning 2005	W/m^2	-1.000	0.000	-0.400
36	RF_VOLCANIC_SCALE	GL	Scaling factor for volcanic forcing		0.000	1.000	0.660
37	STRATOZ_CLEXPON	GL	Dependency of strat. ozone on EESC concentrations		1.000	3.000	2.000
38	STRATOZ_O3SCALE	GL	Scaling factor for strat. ozone depletion		-0.003	0.001	-0.001
39	TROPOZ_OZCH4	GL	Sensitivity of trop. ozone on methane abundance changes	DU/ppb	1.000	10.000	5.000
40	TROPOZ_OZCO	GL	Sensitivity of trop. ozone on CO abundance changes	DU/Mt	0.000	0.002	0.001
41	TROPOZ_OZVOC	GL	Sensitivity of trop. ozone on NMVOC abundance changes	DU/Mt	0.000	0.007	0.003
42	TROPOZ_RADEFF_WM2PERDU	GL	Radiative forcing efficiency of trop. ozone	$W/m^2/DU$	0.020	0.080	0.034

Table S1 (continued).

No.	Parameter	Region	Description	Min	Max	Standard
Radiative Forcing Pattern Parameters (W/m^2)						
43	RF_REGIONS_CH4	NO	Methane; rel. forcing in NO region	0.484	0.591	0.537
44	RF_REGIONS_CH4	NL	Methane; rel. forcing in NL region	0.392	0.479	0.435
45	RF_REGIONS_CH4	SO	Methane; rel. forcing in SO region	0.540	0.660	0.600
46	RF_REGIONS_CH4	SL	Methane; rel. forcing in SL region	0.364	0.445	0.405
47	RF_REGIONS_CH4OXSTRATH2O	NO	Strat H_2O due to Methane; rel. forcing in NO region	0.036	0.043	0.040
48	RF_REGIONS_CH4OXSTRATH2O	NL	Strat H_2O due to Methane; rel. forcing in NL region	0.044	0.054	0.049
49	RF_REGIONS_CH4OXSTRATH2O	SO	Strat H_2O due to Methane; rel. forcing in SO region	0.078	0.096	0.087
50	RF_REGIONS_CH4OXSTRATH2O	SL	Strat H_2O due to Methane; rel. forcing in SL region	0.038	0.047	0.043
51	RF_REGIONS_CLOUD_ALBEDO	NO	Ind. aerosol rel. forcing in NO region	-1.062	-0.869	-0.966
52	RF_REGIONS_CLOUD_ALBEDO	NL	Ind. aerosol rel. forcing in NL region	-1.539	-1.260	-1.399
53	RF_REGIONS_CLOUD_ALBEDO	SO	Ind. aerosol rel. forcing in SO region	-0.376	-0.308	-0.342
54	RF_REGIONS_CLOUD_ALBEDO	SL	Ind. aerosol rel. forcing in SL region	-0.691	-0.566	-0.628
55	RF_REGIONS_CO2	NO	CO_2; rel. forcing in NO region	1.268	1.550	1.409
56	RF_REGIONS_CO2	NL	CO_2; rel. forcing in NL region	1.233	1.507	1.370
57	RF_REGIONS_CO2	SO	CO_2; rel. forcing in SO region	1.290	1.577	1.433
58	RF_REGIONS_CO2	SL	CO_2; rel. forcing in SL region	1.199	1.466	1.333
59	RF_REGIONS_DUST	NO	Mineral dust; rel. forcing in NO region	-0.895	-0.732	-0.814
60	RF_REGIONS_DUST	NL	Mineral dust; rel. forcing in NL region	-1.669	-1.365	-1.517
61	RF_REGIONS_DUST	SO	Mineral dust; rel. forcing in SO region	-0.360	-0.295	-0.328
62	RF_REGIONS_DUST	SL	Mineral dust; rel. forcing in SL region	-0.695	-0.569	-0.632
63	RF_REGIONS_FGAS	NO	Fluorinated gases; rel. forcing in NO region	0.150	0.184	0.167
64	RF_REGIONS_FGAS	NL	Fluorinated gases; rel. forcing in NL region	0.146	0.178	0.162
65	RF_REGIONS_FGAS	SO	Fluorinated gases; rel. forcing in SO region	0.140	0.171	0.155
66	RF_REGIONS_FGAS	SL	Fluorinated gases; rel. forcing in SL region	0.132	0.161	0.146
67	RF_REGIONS_MHALO	NO	Montreal Protocol gases; rel. forcing in NO region	0.150	0.184	0.167
68	RF_REGIONS_MHALO	NL	Montreal Protocol gases; rel. forcing in NL region	0.146	0.178	0.162
69	RF_REGIONS_MHALO	SO	Montreal Protocol gases; rel. forcing in SO region	0.140	0.171	0.155
70	RF_REGIONS_MHALO	SL	Montreal Protocol gases; rel. forcing in SL region	0.132	0.161	0.146
71	RF_REGIONS_N2O	NO	N_2O; rel. forcing in NO region	0.137	0.168	0.152
72	RF_REGIONS_N2O	NL	N_2O; rel. forcing in NL region	0.126	0.154	0.140
73	RF_REGIONS_N2O	SO	N_2O; rel. forcing in SO region	0.146	0.179	0.162
74	RF_REGIONS_N2O	SL	N_2O; rel. forcing in SL region	0.118	0.144	0.131
75	RF_REGIONS_STRATOZ	NO	Strat. ozone; rel. forcing in NO region	-0.013	-0.011	-0.012
76	RF_REGIONS_STRATOZ	NL	Strat. ozone; rel. forcing in NL region	-0.025	-0.020	-0.023
77	RF_REGIONS_STRATOZ	SO	Strat. ozone; rel. forcing in SO region	-0.069	-0.056	-0.063
78	RF_REGIONS_STRATOZ	SL	Strat. ozone; rel. forcing in SL region	-0.264	-0.216	-0.240
79	RF_REGIONS_TROPOZ	NO	Trop. ozone; rel. forcing in NO region	0.419	0.512	0.466
80	RF_REGIONS_TROPOZ	NL	Trop. ozone; rel. forcing in NL region	0.465	0.568	0.516
81	RF_REGIONS_TROPOZ	SO	Trop. ozone; rel. forcing in SO region	0.159	0.195	0.177
82	RF_REGIONS_TROPOZ	SL	Trop. ozone; rel. forcing in SL region	0.214	0.262	0.238

Table S2 | Constraints applied in this study.

Constrained variable	Region	Range	Unit	Distribution	Source
Air Surface Temperature Constraint, 1850 to 2006					
Air Surface Temperature	NO	see text	K	see text	Brohan et al. (2006)[2]; see hadobs.metoffice.com/hadsst2/diagnostics/time-series.html and hadobs.metoffice.com/crutem3/diagnostics/time-series.html
Air Surface Temperature	NL	see text	K	see text	
Air Surface Temperature	SO	see text	K	see text	
Air Surface Temperature	SL	see text	K	see text	
Ocean Heat Uptake Constraint, 1961 to 2003 (1-sigma range)					
Heat uptake <700m trend (1961 to 2003)	GL	+0.3721 [+-0.0698]	10E22 J/yr	normal	Domingues et al. (2008)[4]
Radiative Forcing Constraints, Year 2005 (90% range uncertainties)					
Carbon Dioxide (CO2_RF)	GL	+1.66 [+-0.17]	W/m^2	normal	Forster et al. (2007), Table 2.12[6]
Methane (CH4_RF)	GL	+0.48 [+-0.05]	W/m^2	normal	
Nitrous Oxide (N2O_RF)	GL	+0.16 [+-0.02]	W/m^2	normal	
Ind. aerosol forcing (CLOUD_TOT_RF)	GL	-0.70 [-1.10,+0.40]	W/m^2	skewed normal	
Direct aerosol forcing (SOXI_RF)	GL	-0.40 [+-0.2]	W/m^2	normal	
Direct biomass buring aerosol (BIOMASSAER_RF)	GL	+0.03 [+-0.12]	W/m^2	normal	
Methane induced strat. H2O (CH4OXSTRATH2O_RF)	GL	+0.07 [+-0.05]	W/m^2	normal	
All halogenated gases (HALOSUM_RF)	GL	+0.34 [+-0.03]	W/m^2	normal	
Strat. ozone (STRATOZ_RF)	GL	-0.05 [+-0.10]	W/m^2	normal	
Trop. ozone (TROPOZ_RF)	GL	+0.35 [-0.10, +0.3]	W/m^2	skewed normal	
Solar forcing (SOLAR_RF)	GL	+0.12 [-0.06, +0.18]	W/m^2	skewed normal	
Direct nitrate aerosol (NOXI_RF)	GL	-0.10 [+-0.10]	W/m^2	normal	
Direct fossil fuel aerosol BC (BCI_RF)	GL	+0.2 [+-0.15]	W/m^2	normal	
Direct fossil fuel aerosol, organic carbon (OCI_RF)	GL	-0.05 [+- 0.05]	W/m^2	normal	
Direct mineral dust aerosol (MINERALDUST_RF)	GL	-0.10 [+-0.20]	W/m^2	normal	
Surface albedo, landuse (LANDUSE_RF)	GL	-0.20 [+-0.20]	W/m^2	normal	
Surface albedo, BC aerosol on snow (BCSNOW_RF)	GL	+0.10 [+-0.10]	W/m^2	normal	
Change of effective climate sensitivity between 20th and 21st century under SRES A1B scenario (Ratio over means across 2050-2100 and 1950-2000) (90% range)					
Ratio of effective climate sensitivity (DAT_CLIMSENS_EFF)	GL	1.23 [1.06 to 1.51]	K/K	skewed normal	Own calculations based on 190 CMIP3 & C4MIP emulations as described in Meinshausen et al. (2008)[1]

Table S3 | Median and 80% range estimates of potential CO_2 emissions arising from burning all proven recoverable reserves of fossil fuels (see text).

	Potential Emissions ($GtCO_2$)		
Proven Recoverable Reserve	**Median (50%)**	**Lower (10%)**	**Upper (90%)**
Natural Gas	**360**	**345**	**379**
Oil (conventional)	497	465	530
Oil (non-conv.)	118	64	175
Oil total	**615**	**553**	**680**
Coal (bituminous & anthracite)	1,126	952	1,333
Coal (sub-bituminous)	482	353	615
Coal (lignite)	192	114	332
Coal total	**1,820**	**1,569**	**2,106**
Total	**2,800**	**2,541**	**3,089**

Table S4 | Distributions of climate sensitivity and transient climate response as shown in Figure 1.

Label	Study	Ref.	Remarks
Climate Sensitivity			
1	Forest et al. (2002)	37	Expert Prior
2	Frame et al. (2005)	38	Uniform Prior on Observables
3	Frame et al. (2005)	38	Uniform Prior on Climate Sensitivity
4	Forster & Gregory (2006)	39	Derived from Earth Radiation Budget
5	Wigley & Raper (2001)	40	Lognormal proxy of IPCC TAR ranges
6	Forest et al. (2002)	37	Uniform Prior on Climate Sensitivity
7	Gregory et al. (2002)	9	
8	Hegerl et al. (2006)	7	
9	Annan & Hargreaves (2006)	41	Combination literature studies
10	Forest et al. (2006)	42	No Expert Prior
11	Knutti et al. (2005)	11	Climateprediction.net
12	Knutti et al. (2002)	43	
13	Andronova & Schlesinger (2001)	10	Combination of those PDFs that including nat. radiative forcing.
14	Piani et al. (2005)	12	Climateprediction.net
15	Forest et al. (2006)	42	Expert Prior
16	Frame et al. (2006)	13	Uniform Prior on TCR
17	Murphy et al. (2004)	44	Weighted distribution
18	Tomassini et al. (2007)	14	Expert Prior
19	Tomassini et al. (2007)	14	Uniform Prior
Transient Climate Response			
20	Knutti & Tomassini (2008)	45	Expert Prior
21	Knutti & Tomassini (2008)	45	Uniform Prior
22	Stott et al. (2006)	46	Based on HadCM3
23	Stott et al. (2006)	46	Based on GFDL R30
24	Stott et al. (2006)	46	Based on PCM
25	Frame et al. (2006)	13	Uniform Prior on TCR

ADDITIONAL REFERENCES

1 Meinshausen, M., Raper, S. C. B. & Wigley, T. M. L. Emulating IPCC AR4 atmosphere-ocean and carbon cycle models for projecting global-mean, hemispheric and land/ocean temperatures: MAGICC 6.0. *Atmospheric Chemistry and Physics Discussions* **8**, 6153–6272 (2008).

2 Brohan, P., Kennedy, J. J., Harris, I., Tett, S. F. B. & Jones, P. D. Uncertainty estimates in regional and global observed temperature changes: A new data set from 1850. *Journal of Geophysical Research-Atmospheres* **111**, D12106, doi:10.1029/2005JD006548 (2006).

3 Allen, M. R. & Tett, S. F. B. Checking for model consistency in optimal fingerprinting. *Climate Dynamics* **15**, 419-434 (1999).

4 Domingues, C. M., Church, J. A., White, N. J., Gleckler, P. J., Wijffels, S. E., Barker, P. M. & Dunn, J. R. Improved estimates of upper-ocean warming and multi-decadal sea-level rise. *Nature* **453**, 1090-U1096 (2008).

5 Levitus, S., Antonov, J. & Boyer, T. Warming of the world ocean, 1955-2003. *Geophysical Research Letters* **32**, L02604 (2005).

6 Forster, P., Ramaswamy, V., Artaxo, P., Berntsen, T., Betts, R., Fahey, D. W., Haywood, J., Lean, J., Lowe, D. C., Myhre, G., Nganga, J., Prinn, R., Raga, G., Schulz, M. & Van Dorland, R. in *Climate Change 2007: The Physical Science Basis. Contribution of Working Group I to the Fourth Assessment Report of the Intergovernmental Panel on Climate Change* (eds S. Solomon *et al.*), pp. 129-234 (Cambridge University Press, 2007).

7 Hegerl, G. C., Crowley, T. J., Hyde, W. T. & Frame, D. J. Climate sensitivity constrained by temperature reconstructions over the past seven centuries. *Nature* **440**, 1029-1032 (2006).

8 Knutti, R., Stocker, T. F., Joos, F. & Plattner, G. K. Probabilistic climate change projections using neural networks. *Climate Dynamics* **21**, 257-272 (2003).

9 Gregory, J. M., Stouffer, R. J., Raper, S. C. B., Stott, P. A. & Rayner, N. A. An observationally based estimate of the climate sensitivity. *Journal of Climate* **15**, 3117-3121 (2002).

10 Andronova, N. G. & Schlesinger, M. E. Objective estimation of the probability density function for climate sensitivity. *Journal of Geophysical Research-Atmospheres* **106**, 22605-22611 (2001).

11 Knutti, R., Meehl, G. A., Allen, M. R. & Stainforth, D. A. Constraining climate sensitivity from the seasonal cycle in surface temperature. *Journal of Climate* **19**, 4224-4233 (2006).

12 Piani, C., Frame, D. J., Stainforth, D. A. & Allen, M. R. Constraints on climate change from a multi-thousand member ensemble of simulations. *Geophysical Research Letters* **32**, L23825 (2005).

13 Frame, D. J., Stone, D. A., Stott, P. A. & Allen, M. R. Alternatives to stabilization scenarios. *Geophysical Research Letters* **33**, L14707, doi:10.1029/2006GL025801 (2006).

14 Tomassini, L., Reichert, P., Knutti, R., Stocker, T. F. & Borsuk, M. E. Robust Bayesian uncertainty analysis of climate system properties using Markov chain Monte Carlo methods. *Journal of Climate* **20**, 1239-1254 (2007).

15 IPCC. Climate Change 2007: Mitigation. Contribution of Working Group III to the Fourth Assessment Report of the Intergovernmental Panel on Climate Change. pp. 860 (Cambridge University Press, Cambridge, UK and New York, USA, 2007).

16 Hansen, J., Sato, M., Ruedy, R., Nazarenko, L., Lacis, A., Schmidt, G. A., Russell, G., Aleinov, I., Bauer, M., Bauer, S., Bell, N., Cairns, B., Canuto, V., Chandler, M., Cheng, Y., Del Genio, A., Faluvegi, G., Fleming, E., Friend, A., Hall, T., Jackman, C., Kelley, M., Kiang, N., Koch, D., Lean, J., Lerner, J., Lo, K., Menon, S., Miller, R., Minnis, P., Novakov, T., Oinas, V., Perlwitz, J., Perlwitz, J., Rind, D., Romanou, A., Shindell, D., Stone, P., Sun, S., Tausnev, N., Thresher, D., Wielicki, B., Wong, T., Yao, M. & Zhang,

S. Efficacy of climate forcings. *Journal Of Geophysical Research-Atmospheres* **110**, D18104, doi:10.1029/2005JD005776 (2005).

17 Meinshausen, M., Hare, B., Wigley, T. M. L., van Vuuren, D., den Elzen, M. G. J. & Swart, R. Multi-gas emission pathways to meet climate targets. *Climatic Change* **75**, 151-194, doi:10.1007/s10584-005-9013-2 (2006).

18 Wigley, T. M. L. Could reducing fossil-fuel emissions cause global warming? *Nature* **349**, 503-506 (1991).

19 World Energy Council. Survey of Energy Resources 2007. pp. 600 (World Energy Council, London United Kingdom, 2007).

20 BP. BP Statistical Review of World Energy. pp. 48 (BP, London, 2008).

21 BGR. Reserves, Resources and Availability of Energy Resources 2006. pp. 92 (German Federal Institute for Geosciences and Natural Resources, Hannover, Germany, 2007).

22 IPCC. 2006 Guidelines for National Greenhouse Gas Inventories. pp. 1988 (IPCC National Greenhouse Gas Inventories Programme, Hayama, Japan, 2006).

23 Energy Information Administration. *International Energy Annual; Unpublished file data of the Coal Reserves Data Base (April 2007), as cited on www.eia.doe.gov/aer/txt/stb1113.xls*, 2007).

24 Abraham, K. International Outlook: World Trends, Operators ride the crest of the global wave. *World Oil* **228** (2007).

25 WEC. *2007 Survey of Energy Resources*. pp. 600 (World Energy Council, 2007).

26 PennWell Corporation. SPECIAL REPORT: Oil production, reserves increase slightly in 2006. *Oil & Gas Journal* **104**, 20-23 (2006).

27 Nakicenovic, N. & Swart, R. IPCC Special Report on Emissions Scenarios. pp. 612 (Cambridge University Press, Cambridge, United Kingdom, 2000).

28 WMO. Scientific Assessment of Ozone Depletion: 2006. pp. 572 (World Meteorological Organization, Geneva, Switzerland, 2006).

29 Council of the European Union. Presidency conclusions - Brussels, 22/23 March 2005 pp. 39 (European Commission, 2005).

30 ENB. COP14 Highlights. *Earth Negotiations Bulletin* (2008). <http://www.iisd.ca/vol12/enb12394e.html>.

31 Stoltenberg, J. Speech at UN Climate Change Conference in Bali, 13.Dec.2007 pp. 2 (Government of Norway, 2007).

32 van Schalkwyk, M. Climate Change: Extinction Threat Necessitates Definitive Action, 21 July 2008 pp. 2 (Government of South Africa, 2008).

33 Switzerland. Vernehmlassungsvorlage zur Revision des CO_2-Gesetzes pp. 113 (Eidgenössisches Departement für Umwelt, Verkehr, Energie und Kommunikation UVEK, 2008).

34 Iceland. Bali Action Plan pp. 25-28 (United Nations Framework Convention on Climate Change, 2008).

35 Costa Rica, El Salvador, Honduras, Nicaragua & Panama. The Bali Action Plan: Suggestion to move forward pp. 5 (United Nations Framework Convention on Climate Change, 2008).

36 UN. *World Population Prospects: The 2006 Revision Population Database*, <http://esa.un.org/unpp> (2007).

37 Forest, C. E., Stone, P. H., Sokolov, A., Allen, M. R. & Webster, M. D. Quantifying Uncertainties in Climate System Properties with the Use of Recent Climate Observations. *Science* **295**, 113-117 (2002).

38 Frame, D. J., Booth, B. B. B., Kettleborough, J. A., Stainforth, D. A., Gregory, J. M., Collins, M. & Allen, M. R. Constraining climate forecasts: The role of prior assumptions. *Geophysical Research Letters* **32**, L09702, doi:10.1029/2004GL022241 (2005).

39 Forster, P. M. D. & Gregory, J. M. The climate sensitivity and its components diagnosed from Earth Radiation Budget data. *Journal of Climate* **19**, 39-52 (2006).

40 Wigley, T. M. L. & Raper, S. C. B. Interpretation of high projections for global-mean warming. *Science* **293**, 451-454 (2001).

41 Annan, J. D. & Hargreaves, J. C. Using multiple observationally-based constraints to estimate climate sensitivity. *Geophysical Research Letters* **33**, L06704 (2006).

42 Forest, C. E., Stone, P. H. & Sokolov, A. P. Estimated PDFs of climate system properties including natural and anthropogenic forcings. *Geophysical Research Letters* **33**, L01705 (2006).

43 Knutti, R., Stocker, T. F., Joos, F. & Plattner, G. K. Constraints on radiative forcing and future climate change from observations and climate model ensembles. *Nature* **416**, 719-723 (2002).

44 Murphy, J. M., Sexton, D. M. H., Barnett, D. N., Jones, G. S., Webb, M. J., Collins, M. & Stainforth, D. A. Quantification of modelling uncertainties in a large ensemble of climate change simulations. *Nature* **430**, 768-772 (2004).

45 Knutti, R. & Tomassini, L. Constraints on the transient climate response from observed global temperature and ocean heat uptake. *Geophysical Research Letters* **35**, L09701 (2008).

46 Stott, P. A., Mitchell, J. F. B., Allen, M. R., Delworth, T. L., Gregory, J. M., Meehl, G. A. & Santer, B. D. Observational constraints on past attributable warming and predictions of future global warming. *Journal of Climate* **19**, 3055-3069 (2006).